# *SECTION 3*

# THERMAL AND FAST REACTOR MATERIALS

UDC 669-1:51-74:519.257

# FORECASTING OF STRUCTURAL TRANSFORMATIONS IN HEAT AFFECTED ZONE STEEL OF 15Kh2NMFA AT ANTI-CORROSION CLADDING

***L.M. Lobanov, V.A. Kostin, O.V. Makhnenko, V.V. Zukov, E.S. Kostenevich***
***E.O. Paton Electric Welding Institute of the NAS of Ukraine, Kyiv, Ukraine***
***E-mail: valerykkos@gmail.com; makhnenko@paton.kiev.ua***

Using mathematical modeling based on existing parametric regression equations the prediction of microstructure-phase transformations in heat affected zone( HAZ) metal of base material (steel 15Kh2NMFA) of WWER-1000 reactor vessel in arc cladding of protective anti-corrosion layer was carried out as well as performed comparative analysis of modeling results with obtained experimental data of dilatometric and metallographic analysis. The comparison of results ensures formation of bainite-martensite structure in HAZ metal of WWER-1000 reactor vessel, however a value of content of martensite in calculation and experimental determination is different on ~ 40…50%. To clarify the calculated results, a thermokinetic diagram of the decomposition of supercooled austenite was constructed for characteristic cooling rates (3; 4, and 5 °C/s) during the welding/surfacing thermal cycle. As a result, adequate parameters of the microstructure-phase composition in the HAZ of steel 15Kh2NMFA at corrosion-resistant cladding were obtained.

## INTRODUCTION

Nuclear power occupies a leading position in the production of electricity in Ukraine. Most nuclear power plants are of the type WWER-1000, reactor pressure vessels (RPV) of which is made of thick-wall forged shells of low-alloy high-strength steels of pearlite class of 15Kh2NMFA grade, welded by girth welds. To protect the RPV from corrosion, austenitic material was deposited on the inner surface. Currently, most reactors of this type have already reached an assigned resource for safe operation. Therefore, an important scientific and technical task is to assess the possibility of extending the resource of their safe operation. To justify the extension of the RPV service life, it is necessary to take into account the residual stresses resulting from welding or cladding heating, and their redistribution in the further process of heat treatment.

Technological parameters of process of anti-corrosion cladding can have significant effect on microstructure-phase composition in melting zone (MZ) and heat-affected zone (HAZ) of 15Kh2NMFA pearlitic steel, as well as on distribution of residual stresses in WWER-1000 RPV. For a reliable calculated prediction of the residual stresses in the cladding zone of RPV, it is necessary to take into account the structural-phase composition formed in the HAZ.

Analysis of open access references shows [1–7] that there are not exact data on microstructure-phase composition of the RPV steel after arc cladding as well as there is no it's complete CCT diagram of overcooled austenite decomposition.

Existing metallurgical CCT diagrams of RPV steels [8, 9], obtained for typical at heat treatment procedure long-term holdings at maximum temperature and low cooling rates, do not allow to determine a final microstructure-phase composition of metal in HAZ due to peculiarities of welding/cladding thermal cycle.

There are data [10] that there is formation of bainite-martensite microstructure in HAZ metal at cooling rate 3.3…28 °C/s in 800…500 °C temperature range for steel 15Kh2NMFA and critical cooling rate, above which completely martensite structure is formed in HAZ metal, makes 30 °C/s. The results, obtained in work [11], vice versa, show that typical welding thermal cycle with cooling rate 3…6 °C/s can produce the formation of mainly martensite microstructure. In the atlases and collections of CCT diagrams [12–14] also there are no data for steel 15Kh2NMFA at heat treatment and welding/cladding.

New data [15–17] on transformations in RPV steels 15Kh2MFA-A and 15Kh2NMFA under conditions of different thermal cycles of cooling have been presented recently, analysis of which showed presence of specific differences of temperatures of start and end of phase transformations, critical cooling rates and fractions of structural constituents. These differences, apparently, are related, on the one hand, with little various chemical composition of researched reactor vessel steels, and on the other hand, with difference of methods (devices), used for determination of temperature phase transformations, including dimensions of samples and duration of holding in austenite temperature range [15–17].

In recent times, the mathematical models got a large development for prediction of phase composition of structural steels at thermal effect [18–21]. The objectives of the current work are determination of possibility of application of mathematical modeling of kinetics of microstructure transformations in HAZ metal of WWER-1000 RPV during arc cladding taking into account different technological parameters and conducting of experimental validation of the calculation results using physical modeling of thermal-deformation state at welding/cladding by Gleeble 3800.

## TECHNOLOGY, MATERIAL AND RESEARCH METHODS

In accordance with the requirements of normative documentation [22], corrosion-resistant coatings of the RPV should be performed using automatic arc cladding with submerged arc welding strip (Fig. 1), or manual arc cladding with coated electrodes or argon-arc cladding.

*Fig. 1. Submerged arc welding using a strip electrode*

In accordance to reference document [23] automatic submerged-arc cladding with strip electrodes was used for cylinder part of RPV and manual arc cladding with coated electrodes was used for surface of nozzle zone (inner surface of Du850 nozzle and their fillets) whereas other difficult-to-weld places of vessel – by manual arc surfacing with coated electrodes.

The technological parameters for automatic submerged-arc cladding by strips were the following [24–27], namely: current $I_w$=650 A, voltage $U_a$=32 V, width of strip electrode 60 mm, temperature of preheating and concurrent heating $T_h$=250 °C, cladding rate $v_c$=10 m/h. Technological parameters for manual arc cladding with coated electrodes: current $I_w$=130…150 A, voltage $U_a$=26…30 V, electrode diameter 4–5 mm, temperature of preliminary and concurrent heating $T_h$=250 °C, cladding rate $v_s$=3 m/h. Composition of base material of steel 15Kh2NMFA is presented in [28].

Chemical composition of 15Kh2NMFA steel samples (Table 1) was determined on atomic emission spectrometer with inductively-coupled plasma ICAP 6500 DUO (TERMO FISHER SCIENTIFIC, USA). Content of carbon was determined by coulombometric method. Thermal-physical properties of base metal and RPV cladding consumables depending on temperature are given in works [29, 30].

To verify the results of mathematical modeling of the microstructural composition of the HAZ metal 15Kh2NMFA steel after arc cladding physical modeling was carried out on a Gleeble 3800. CCT thermokinetic diagrams of austenite decomposition were plotted at different cooling rates of 1; 3; 5; 7 °C/s. Microstructure of samples were studied by optical metallographic microscope Neophot-32 (Japan), scanning JSM 840 (JEOL, Japan) and transmission JEOL 200CX (JEOL, Japan) electron microscope. Vickers hardness measurement was performed on hardness gauge M-400 of LECO Company at 100 g and 1 kg loading.

## MATHEMATICAL MODEL

Mathematical modeling was carried out on a finite-element model of nozzle zone of WWER-1000 RPV, cladding of which was performed on both mentioned above technologies. Two types of cladding heating source were used: strip source for cylindrical vessel shell and spot source, simulating manual cladding with coated electrodes, for inner surface of nozzle.

A temperature problem was solved in 2D formulation at assumption of fast moving heat source and axial symmetry of cladding of protective layers with respect of axis of cylindrical RPV shell or axis of nozzle at boundary condition of convective heat exchange with environment. Distribution of heat power of strip source $W_1$ and spot source $W_2$ with 2D formulation in a cylindrical coordinate system can be described by dependencies (1) and (2), respectively:

$$W_1(r,z,t)=\frac{2\cdot Q\cdot\sqrt{K_r\cdot K_z}}{\pi\cdot v\cdot t_н\cdot\left[1+\sqrt{\frac{K_z}{\pi}}b\right]}\cdot\exp\left[-K_r D_r{}^2-K_z D_z{}^2\right], \quad (1)$$

$$W_2(r,z,t)=\frac{2\cdot Q\cdot\sqrt{K_r\cdot K_z}}{\pi\cdot v\cdot t_н}\cdot\exp\left[-K_r D_r{}^2-K_z D_z{}^2\right], \quad (2)$$

where $D_z=z-z_0$; $D_r=r-r_0$; $r$, $z$ – coordinates (radial and axial) of considered point of the nozzle zone; $r_0$, $z_0$ – coordinates of a center of moving heat source; $K_r$; $K_z$ – coefficients of concentration of specific heat flow; $t_h$ – heating time; $Q$ – effective power of heating source ($Q=\mu I_w U_a$); $\mu$ – efficiency coefficient; $v$ – cladding rate; $b$ – strip electrode width.

Table 1

Composition of examined steel 15Kh2NMFA

| | Chemical composition steel, *wt.%* | | | | | | | | | |
|---|---|---|---|---|---|---|---|---|---|---|
| | C | Si | Mn | Cr | Ni | Mo | Cu | V | S | P |
| Sample | 0.17 | 0.28 | 0.41 | 2.04 | 1.37 | 0.63 | 0.03 | 0.12 | 0.01 | 0.01 |
| Standard TU 108-765-78 [28] | 0.13… 0.18 | 0.17… 0.37 | 0.3… 0.6 | 1.8… 2.3 | 1.0… 1.5 | 0.5… 0.7 | ≤ 0.3 | 0.10… 0.12 | ≤0.02 | ≤ 0.02 |

Note. Base – iron. Content of elements shall not exceed, wt.%: Co ≤ 0.03; As ≤ 0.04. For steel 15Kh2NMFA-A content of elements shall not exceed, wt.%: Sn ≤ 0.005; Sb ≤ 0.005; Cu ≤ 0.10; S ≤ 0.012; P ≤ 0.010; As ≤ 0.010.

Distribution of residual stresses in vessel material depends on microstructure composition and, respectively, on mechanical properties in MZ and HAZ. In accordance with calculation approach [18, 19], based on application of parametric regression equations, the results of calculation of maximum fraction weight of each microstructure phase ($V_m^{\max}$ – martensite; $V_b^{\max}$ – bainite; $V_{fp}^{\max}$ – ferrite-pearlite) in a final structure after cooling depend on chemical composition of steel and typical time $\Delta t_{8/5}$(s) of cooling from 800 to 500 °C and can be defined by formulas (3) – (5):

$$V_m^{\max} = 0,5\left[1 - erf\,\frac{\ln \Delta t_{8/5} - \ln \Delta t_m^{50}}{\ln S_m}\right]; \quad (3)$$

$$V_{pf}^{\max} = 0,5\left[1 + erf\,\frac{\ln \Delta t_{8/5} - \ln \Delta t_{fp}^{50}}{\ln S_{fp}}\right]; \quad (4)$$

$$V_b^{\max} = 1 - V_m^{\max} - V_{fp}^{\max}, \quad (5)$$

where $\Delta t_m^{50}$ is the time (s) of cooling from 800 to 500 °C temperature, at which in microstructure after cooling there is formation of 50 % of martensite ($V_m^{\max}$=0.5); $\Delta t_{fp}^{50}$ is the time (s) of cooling from 800 to 500 °C temperature, at which in microstructure after cooling there is formation of 50% of ferrite-pearlite ($V_{fp}^{\max}$); $S_m$, $S_{fp}$ are the parameters of model of austenite decay.

Values of parameters $\Delta t_m^{50}$, $\Delta t_{fp}^{50}$, $S_m$, $S_{fp}$ for low-alloy steels are determined according to data of work [18].

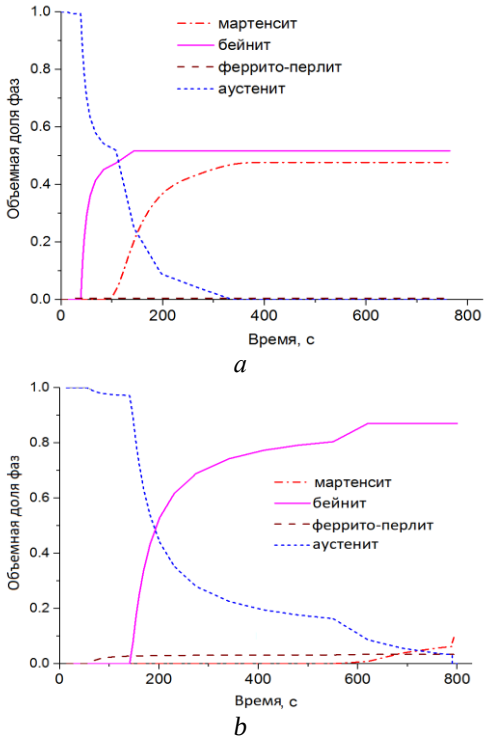


*Fig. 2. The results of the calculated prediction of the kinetics of the decomposition of austenite in HAZ during arc surfacing: a – manual arc surfacing with coated electrodes; b – automatic submerged-arc welding with tape b = 60 mm*

Results of calculation for two technologies of arc cladding showed (Fig. 2) that automatic submerged arc cladding with width of strip electrode *b*=60 mm provokes formation of bainite-martensite structure in HAZ, martensite fraction reaches up to 12%. At manual arc cladding with coated electrodes (width of cladded pass *b*=15 mm) fraction of martensite in HAZ reaches 48% due to higher cooling rate.

## PHYSICAL MODELING

To verify the obtained calculated results experiments on physical modeling on Gleeble 3800 of thermal cycles of cladding for samples from 15Kh2NMFA steel were conducted and a study of their microstructure was carried out. In the process of modeling on the Gleeble 3800 several modes of thermal cycles were simulated: at constant cooling rates with and without exposure at the maximum temperature of the thermal cycle, with cooling according to the real thermal cycle of cladding at different maximum temperatures without prolonged exposure.

In physical modeling of a thermal cycle with a long exposure during heating samples were heated to 1000°C per 10 min, hold at 1000 °C temperature for 170 min, that made the total time of heating 180 min, and next cooling at constant rate 1; 3; 5; 7 °C/s. Dilatometric data recorded during process of thermal effect were used for construction of the CCT diagram of overcooled austenite decomposition (Fig. 3).

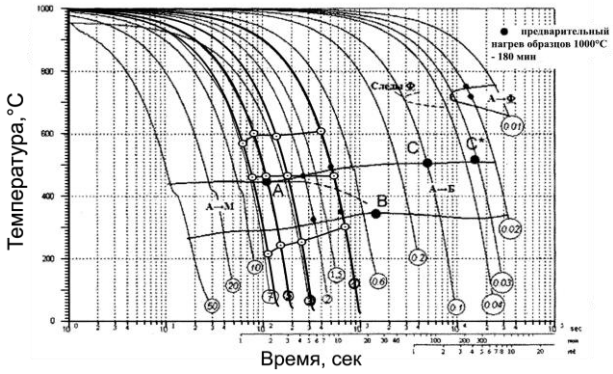


*Fig. 3. Comparison of the constructed ( Θ ) and existing [15] CCT diagram of austenite decomposition of steel 15Kh2NMFA-A*

A comparative analysis of the constructed and existing [15] CCT diagrams of 15Kh2NMFA steel showed that they are slightly different. The differences lie in the presence of a high-temperature region of bainitic transformation within all studied cooling rates. The temperatures of the onset of bainitic transformation in the existing CCT reach 500-510 °C for low cooling rates, while in the constructed diagram the temperature of the onset of bainitic transformation reaches 607 °C for a cooling rate of 1 °C/s.

The results of metallographic studies of samples at cooling rates of 1; 3; 5; 7 ° C/s are presented in Fig. 4. Obtained results showed (Table 2) that as the cooling rate increases, the proportion of martensite in the sample structure increases from 8 % to 80 % (by structural analysis) or from 26 to 66 % (by Gleeble). and the

hardness of HV1 increases from 3530…3780 to 4700…4820 MPa.

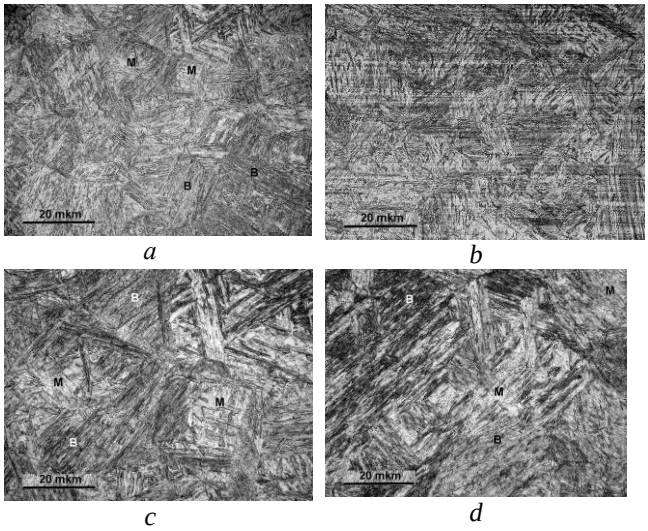


*Fig. 4. Microstructure of 15Kh2NMFA steel samples at cooling speed: a – 1 °C/s; b – 3 °C/s; c – 5 °C/s; d – 7 °C/s. x500*

Table 2

Results of metallographic analysis

| Cooling rate $w_{8/5}$, °C/s | Vickers hardness HV1, MPa | A | B |
|---|---|---|---|
| 1 | 3530…3780 | 92/8 | 74/26 |
| 3 | 4070…4670 | 37/63 | 44/55 |
| 5 | 4390…4760 | 32/68 | 41/59 |
| 7 | 4700…4820 | 20/80 | 34/66 |

Note: A – fraction of bainite/martensite on results of structure analysis (%); B – fraction of bainite/martensite on results of Gleeble analysis (%).

Also a physical simulation of the thermal cycle was carried out without prolonged heating exposure. The proposed thermal regime included heating to 1000 °C, holding at this temperature for a duration of 1 s and subsequent cooling at a constant speed of 5 °C/s.

The analysis showed a sufficiently good correspondence of the obtained and existing data [15] on the transformation temperatures in steel 15Kh2NMFA during the thermal cycle without a long holding time with a constant cooling rate of 5 °C/s. Thus, the temperatures of the onset of the martensitic transformation of 452 °C and the end of the martensitic transformation of 320 °C correspond well to the similar temperatures at the CCT presented in [15], which at a given cooling rate are 445 and 300 °C, respectively. The results of quantitative microstructure analysis confirmed the formation of ~ 100 % martensitic structure (Fig. 5).

In a real cladding process metal cooling does not occur linearly, therefore, physical modeling of characteristic thermal welding/cladding cycles (preheating temperature $T_p$=250 °C) was carried out for 15Kh2NMFA steel samples with different cooling rates in the temperature range 800...500°C (3; 4; 5 °C/s) and at two different maximum heating temperatures (1000 and 1350 °C). Table 3 shows the maximum fractions of the microstructural phases and transformation temperatures under the conditions of a real thermal cycle of welding/cladding for steel 15Kh2NMFA.

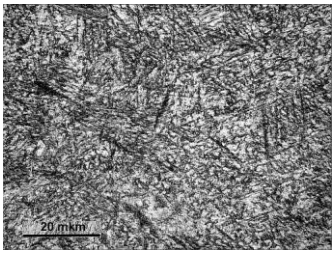


*Fig. 5. Microstructure of 15H2NMFA steel sample at 5 °C/s without long exposure, x500*

Metallographic studies of samples after modelling on the Gleeble 3800 real thermal cycles of cladding at a cooling rate of 5 °C/s (in the temperature range 800...500 °C), differing in the maximum heating temperature, are presented in Fig. 6.

The structure of the sample obtained by the real thermal cycle of welding with a maximum heating temperature of 1000 °C is characterized by a banded inhomogeneous structure consisting of alternating strips of dispersed fine-needle martensite (80 %) and coarse-needle structure of lower bainite (20 %) (see Fig. 6,a).

Table 3

Transformation temperatures of 15Kh2NMFA steel under real thermal cycle conditions at cooling rates of 3; 4; 5 °C/s

| Cooling rate, °C/s_maximum heating temperature,°C | Critical points, °C | | The transformation temperature in the cooling stage,°C | | | Beinite/Martensite, % |
|---|---|---|---|---|---|---|
| | $A_{c1}$ | $A_{c3}$ | $B_s$ | $M_s$ | $M_f$ | |
| 3_1000 | 751 | 885 | 479 | – | 306 | 100/0 |
| 4_1000 | 711 | 881 | 475 | 334 | 273 | 70/30 |
| 5_1000 | 731 | 870 | 457 | – | 308 | 20/80 |
| 3_1350 | 735 | 876 | 491 | – | 324 | 95/5 |
| 4_1350 | 714 | 862 | 481 | 352 | 288 | 90/10 |
| 5_1350 | 714 | 872 | 480 | – | 288 | 0/100 |

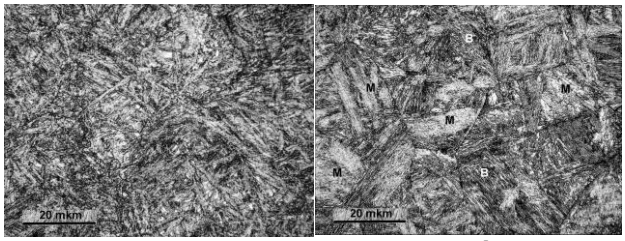


*a* *b*

*Fig. 6. Microstructure of the sample at 5 °C/s, obtained by a real cladding thermal cycle at maximum heating temperatures of 1000 °C (a) and 1350 °C (b), x500*

The sample's structure obtained by the real thermal cycle with a maximum heating temperature of 1350 °C is characterized by a homogeneous martensitic structure (see Fig. 6,b). The size of large martensitic packets is 50 ... 60 microns, and small – 20...30 μm. Vickers hardness HV1 of this structure varies from 4130 to 4530 MPa.

A comparison of the microstructures of the studied samples shows that a change in the maximum heating temperature has almost no effect on the kinetics of the formation of the martensitic phase, does not significantly affect the temperature of the beginning and end of phase formation, but affects the maximum proportion of phases in the final microstructure up to 20%.

## DISCUSSION OF RESEARCH RESULTS

A comparison of the obtained experimental data and the results of mathematical modeling of microstructural transformations during a real cladding cooling cycle shows that the martensite content in the HAZ of 15Kh2NMFA steel is significantly different (the difference is up to 50 %). Therefore, to adequately simulate the kinetics of microstructural transformations in the HAZ metal during corrosion-resistant cladding of the VVER-1000 RPV, it is necessary to use experimental CCT diagram constructed for characteristic welding/cladding thermal cycles.

To carry out mathematical modeling of microstructural transformations in the HAZ of 15Kh2NMFA steel, an averaged CCT diagram of austenite decomposition was constructed for the characteristic thermal welding/cladding cycles (Fig. 7).

Comparison of the constructed CCT diagram with the existing diagrams shows an insignificant difference in the temperatures of the beginning and end of transformations (~ 50 °C), and the main difference is related to the range of martensitic-bainitic transformation and its critical cooling rates.

Point A corresponds to the beginning of the martensitic-bainitic transformation (100 % martensite, according to the existing data cooling rate 5 °C/s), point B – to the end (100 % bainite, cooling rate 0.6 °C/s). These are the so-called "critical" cooling rates in the range of martensitic and bainitic transformations.

According to the obtained results the point A1 corresponds to the critical cooling rate of the martensitic transformation at 5 °C/s and B1 – to the critical cooling rates of the bainitic transformation at 3 °C/s, and this points do not coincide with the literary data (points A and B). Therefore, according to experimental data obtained for real cladding thermal cycles the range of critical transformation rates during welding/cladding is more narrow than that given in existing metallurgical CCT diagrams [8, 9, 15–17].

## CONCLUSIONS

1. A comparative analysis of the calculated and experimental results of the study of phase transformations during anticorrosive cladding of the WWER-1000 reactor pressure vessel showed a significant effect of the technological parameters of the arc cladding process on the kinetics of microstructural transformations and the final phase composition of the HAZ metal of steel 15Kh2NMFA.

2. Using of the calculation method, based on parametric regression equations, allows to predict the phase composition of the HAZ metal for manual arc cladding with coated electrodes (cooling rate 8...9 °C/s) with a maximum martensite content of ~ 50%, and for automatic submerged arc welding with strip electrodes (4...5 °C/s) – the maximum content of martensite is 15%.

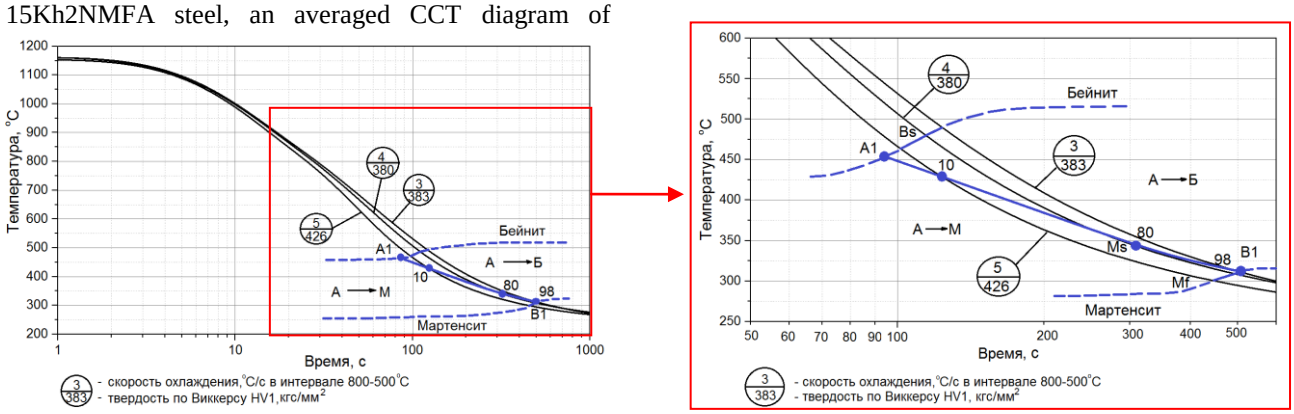


*Fig. 7. TCD of austenite decomposition of steel 15X2NMFA for typical welding cooling cycles*

3. It was experimentally defined that in the studied range of cooling rates of 1...7 °C/s, the final microstructure of the HAZ metal of 15Kh2NMFA steel after prolonged exposure at a temperature of 1000 °C in the austenitic range consists of a bainite-martensitic mixture, and after a short exposure time of ~ 1 s –consists entirely of martensite.

4. The influence of the maximum heating temperature (1000 and 1350 °C) of the sample during the real cladding cooling cycle on the nature of the transformation, microstructure, fraction of the forming phases, and the temperatures of the beginning and end of the formation of bainite and martensite is shown.

5. For adequate modeling of the kinetics of microstructural transformations and the final structural-phase composition in the HAZ during anticorrosive cladding of the VVER-1000 RPV, it is necessary to use experimental CCT diagrams constructed for characteristic welding/surfacing thermal cycles in which there is no long exposure at the austenization temperature. For this purpose, the simplified CCT diagram for 15Kh2NMFA steel, based on the processing of experimental data for two maximum heating temperatures and different cooling rates, is proposed.

## REFERENCES


1. *Нормы расчета на прочность оборудования и трубопроводов атомных энергетических установок (ПНАЭ Г-7-002-86)* / Госатом-энергонадзор СССР. М.: «Энергоатомиздат», 1989, 525 с.

2. А.А. Хлыбов, А.Л. Углов. Определение физико-механических характеристик материала образцов, подвергаемых радиационному облучению // *Труды Нижегородского государственного технического университета им. Р.Е. Алексеева.* 2013, №1(98), с. 220-228.

3. Б.А. Гурович, Е.А. Кулешова, С.В. Федотова. Влияние химического состава и структурных параметров сталей корпусов реакторов ВВЭР на склонность к охрупчиванию, обусловленному образованием зернограничных сегрегаций, в том числе в условиях, характерных для длительной эксплуатации энергетических установок // *Материалы 7-й Межд. науч.-техн. конф. «Обеспечение безопасности АЭС с ВВЭР».* Подольск: ОКБ «Гидропресс», 2011. Эл. ресурс. http://www.gidropress.podolsk.ru/files/proceedings/mntk2011/autorun/article151-ru.htm.

4. А.С. Фролов. *Фазово-структурное состояние и служебные характеристики новых композиций сталей для корпусов реакторов с повышенной мощностью и сроком службы*: Авт. дис. ... канд. техн. наук. М.: Нац. исслед. центр «Курчатовский институт», 2013, 24 с.

5. С.И. Марков. *Металловедческие основы производства заготовок для высоконадежных элементов энергетических и трубопроводных систем*: Авт. дис. ... докт. техн. наук. М.: Центр. науч.-исслед. ин-т технологии машиностроения, 2012, 84 с.

6. Б.З. Марголин, В.А. Швецова, А.Г. Гуленко и др. Прогнозирование трещиностойкости корпусной реакторной стали на основе концепции “Mastercurve” и вероятностной модели // *Проблемы прочности.* 2002, №1, с. 5-21.

7. В.Н. Фоменко. *Прогнозирование вязкости разрушения для расчета прочности корпусов реакторов типа ВВЭР на основе испытаний образцов-свидетелей и локального критерия хрупкого разрушения:* Дис. ... канд. техн. наук. С.-П.: ФГУП «ЦНИИ КМ «Прометей», 2017, 263 с.

8. Л.Е. Попова, А.А. Попов. *Диаграммы превращения аустенита в сталях и бета-растворе в сплавах титана:* Справочник термиста. М.: «Металлургия», 1991.

9. Г.П. Карзов, Б.З. Марголин, И.В. Теплухина, В.А. Пиминов. Материаловедческие аспекты повышения безопасности эксплуатации перспективных ВВЭР на основе совершенствования корпусной стали // *Атомная энергия*. 2016, т. 121, в. 1, с. 25-36.

10. Л.С. Лившиц, А.Н. Хакимов. *Металлове-дение сварки и термическая обработка сварных соединений.* М.: «Машиностроение», 1989, 336 с.

11. Б.З. Марголин, А.Я. Варовин, В.И. Кос-тылев. Определение остаточных напряжений в корпусах реакторов ВВЭР после многопроходной сварки, наплавки и высокотемпературного отпуска // *Автомат. сварка.* 2005, №10(630), с. 16-22.

12. *Atlas of isothermal transformation and cooling transformation diagrams American Society for Metals*. 1977, 432 p.

13. *Atlas of continuous cooling transformation (CCT) diagrams applicable to low carbon low alloy weld metals /* by eds. Z. Zhang and R.A. Farrar. Cambridge, UK. Woodhead, 1995, 100 p.

14. P. Zeyffarth, B. Meyer, A. Scharff. *Grosser Atlas Schweiss-ZTUSchaubilder*. Duesseldorf: DVS-Verlag (in German), 1992, 176 p.

15. *Центр моделирования литейных процес-сов и технологий* (http://mip-cast.ru/treatment).

16. I.V. Teplukhina, V.M. Golod, A.S. Tsvetkov. CCT diagram plotting based on the numerical analysis of dilatometric tests results // *Letters on Materials*. 2018, v. 8(1), p. 37-41.

17. И.В. Соловьев, О.Ю. Корниенко, А.Ю. Жиляков, А.М. Белорусец. Исследование кинетики распада переохлажденного аустенита стали 15Х2НМФА при непрерывном охлаждении // *Материалы XVIII Межд. научно-техн. Уральской школы-семинара металловедов – молодых ученых.* Екатеринбург: УрФУ, 2017, с. 250-252.

18. О.Г. Касаткин, П. Зайффарт. Расчетные модели для оценки механических свойств металла ЗТВ при сварке низколегированных сталей // *Сборник трудов Межд. конф. «Математическое моделирование и информационные технологии в сварке и родственных процессах».* Киев, 2002, с. 103-106.

19. V.I. Makhnenko, E.A. Velikoivanenko, V.E. Pochinok, O.V. Makhnenko, G.Ph. Rozynka, N.I. Pivtorak. Numerical Methods for the Prediction of Welding Stress and Distortions // *Welding and Surfacing Reviews.* 1999, v. 13, Part 1, 146 p.

20. Dean Deng, Yangang Tong, Ninshu Ma, and Hidekazu Murakawa. Prediction of the Residual Welding Stress in 2.25Cr-1Mo Steel by Taking into Account the Effect of the Solid-State Phase Transformations // *Acta Metall. Sin. (Engl. Lett.).* 2013, v. 26, N 3, p. 333-339.

21. Yukio Ueda, Hidekazu Murakawa, Yu Luo. A Computational Model of Phase Transformation for Welding Processes // *Transactions of JWRI*. 1995, v. 24(1), p. 95-100.

22. ПНАЭ Г-7-009-89. *Оборудование и трубопроводы атомных энергетических установок. Сварка и наплавка, основные положения*. М., 2003.

23. *Корпус реактора ЗАЭС-1*. 1152.02.70.000: Паспорт сосуда, работающего под давлением.

24. Т.И. Титова, Н.А. Шульган и др. Совершенствование качества сварных соединений и наплавленных поверхностей оборудования АЭУ производства ОАО «Ижорские заводы» // *Материалы конф. «Обеспечение безопасности АЭС с ВВЭР»,* ОКБ «Гидропресс». С.-Петербург, 2013. Эл.ресурс:http://www.gidropress.podolsk.ru/files/proceedings/mntk2013/autorun/article95ru.htm.

25. Iradj Sattari-Far, Magnus Andersson. *Cladding Effects on Structural Integrity of Nuclear Components*: SKI Report 2006:23, ISSN 1104-1374, ISRN SKI-R-06/23-SE, 73 p.

26. J. Katsuyama, M. Udagawa, H. Nishikawa, M. Nakamura, K. Onizawa. Evaluation of Weld Residual Stress near the Cladding and J-weld in Reactor Pressure Vessel Head for the assessment of PWSCC Behavior // *E-Journal of Advanced Maintenance*. 2010, v. 2, p. 50-64.

27. P. Dupas, D. Moinereau. Evaluation of Cladding Residual Stresses in Clad Blocks by Measurements and Numerical Simulations // *Journal de Physique IV Colloque*. 1996, 06 (C1), p. 187-196; https://hal.archives-ouvertes.fr/jpa-00254150/document.

28. ТУ 108-765-78. *Заготовки из стали марок 15Х2НМФА и 15Х2НМФА-А для корпусов и крышек и других узлов реакторных установок.*

29. V.I. Kostylev, B.Z. Margolin. Determination of residual stress and strain fields caused by cladding and tempering of reactor pressure vessels // *International Journal of Pressure Vessels and Piping*. 2000, v. 77.

30. *Методика определения ресурса корпусов атомных реакторов в процессе эксплуатации* (МРК-СХР-2000), РД ЭО 0353-02. С.-Петербург–Москва, 2000.

*Article received 24.02.2020*

## ПРОГНОЗИРОВАНИЕ СТРУКТУРНЫХ ПРЕВРАЩЕНИЙ В ЗОНЕ ТЕРМИЧЕСКОГО ВЛИЯНИЯ СТАЛИ 15Х2НМФА ПРИ АНТИКОРРОЗИОННОЙ НАПЛАВКЕ

***Л.М. Лобанов, В.А. Костин, О.В. Махненко, В.В. Жуков, Е.С. Костеневич***

Методами математического моделирования на основе параметрических регрессионных уравнений выполнено прогнозирование микроструктурных изменений в металле зоны термического влияния (ЗТВ) стали 15Х2НМФА корпуса реактора ВВЭР-1000 при дуговой наплавке защитного антикоррозионного слоя, а также проведен сравнительный анализ результатов моделирования с полученными экспериментальными данными дилатометрического и металлографического анализов. Сопоставление полученных результатов подтверждает формирование бейнитно-мартенситной структуры в металле ЗТВ корпуса реактора ВВЭР-1000, однако величина содержания мартенсита при расчетном и экспериментальном определении отличается на ~ 40…50%. Для уточнения расчетных результатов была построена термокинетическая диаграмма распада переохлажденного аустенита для характерных скоростей охлаждения (3; 4 и 5 $^{o}$C/c) при сварочном/наплавочном термоцикле. В результате были получены адекватные параметры микроструктуры металла ЗТВ корпусной стали 15Х2НМФА при антикоррозионной наплавке.

## ПРОГНОЗУВАННЯ СТРУКТУРНИХ ПЕРЕТВОРЕНЬ У ЗОНІ ТЕРМІЧНОГО ВПЛИВУ СТАЛІ 15Х2НМФА ПРИ АНТИКОРОЗІЙНОМУ НАПЛАВЛЕННІ

***Л.М. Лобанов, В.А. Костін, О.В. Махненко, В.В. Жуков, О.С. Костеневич***

Методами математичного моделювання на основі параметричних регресійних рівнянь виконано прогнозуванням мікроструктурних перетворень у металі зони термічного впливу (ЗТВ) сталі 15Х2НМФА корпусу реактора ВВЕР-1000 при дуговому наплавленні захисного антикорозійного шару, а також проведено порівняльний аналіз результатів моделювання з отриманими експериментальними даними дилатометричного і металографічного аналізу. Порівняння отриманих результатів підтверджує формування бейнітно-мартенситної структури в металі ЗТВ корпусу реактора ВВЕР-1000, однак вміст мартенситу при математичному та експериментальному моделюванні відрізняється на ~ 40… 50%. Для уточнення розрахункових результатів була побудована термокінетична діаграма розпаду переохолодженого аустеніту для характерних швидкостей охолодження (3, 4 і 5 $^{o}$C/c) при зварювальному/наплавочному термоциклі. В результаті було отримано адекватні параметри мікроструктури металу ЗТВ корпусної сталі 15Х2НМФА при антикорозійному наплавленні.